# Chaos, Strange Attractors, and Fractal Basin Boundaries in Nonlinear Dynamics

CELSO GREBOGI, EDWARD OTT, JAMES A. YORKE

**Recently research has shown that many simple nonlinear deterministic systems can behave in an apparently unpredictable and chaotic manner. This realization has broad implications for many fields of science. Basic developments in the field of chaotic dynamics of dissipative systems are reviewed in this article. Topics covered include strange attractors, how chaos comes about with variation of a system parameter, universality, fractal basin boundaries and their effect on predictability, and applications to physical systems.**

IN THIS ARTICLE WE PRESENT A REVIEW OF THE FIELD OF chaotic dynamics of dissipative systems including recent developments. The existence of chaotic dynamics has been discussed in the mathematical literature for many decades with important contributions by Poincaré, Birkhoff, Cartwright and Littlewood, Levinson, Smale, and Kolmogorov and his students, among others. Nevertheless, it is only recently that the wide-ranging impact of chaos has been recognized. Consequently, the field is now undergoing explosive growth, and many applications have been made across a broad spectrum of scientific disciplines—ecology, economics, physics, chemistry, engineering, fluid mechanics, to name several. Specific examples of chaotic time dependence include convection of a fluid heated from below, simple models for the yearly variation of insect populations, stirred chemical reactor systems, and the determination of limits on the length of reliable weather forecasting. It is our belief that the number of these applications will continue to grow.

We start with some basic definitions of terms used in the rest of the article.

*Dissipative system.* In Hamiltonian (conservative) systems such as arise in Newtonian mechanics of particles (without friction), phase space volumes are preserved by the time evolution. (The phase space is the space of variables that specify the state of the system.) Consider, for example, a two-dimensional phase space ($q$, $p$), where $q$ denotes a position variable and $p$ a momentum variable. Hamilton's equations of motion take the set of initial conditions at time $t = t_0$ and evolve them in time to the set at time $t = t_1$. Although the shapes of the sets are different, their areas are the same. By a dissipative system we mean one that does not have this property (and cannot be made to have this property by a change of variables). Areas should typically decrease (dissipate) in time so that the area of the final set would be less than the area of the initial set. As a consequence of this, dissipative systems typically are characterized by the presence of attractors.

*Attractor.* If one considers a system and its phase space, then the initial conditions may be attracted to some subset of the phase space (the attractor) as time $t \to \infty$. For example, for a damped harmonic oscillator (Fig. 1a) the attractor is the point at rest (in this case the origin). For a periodically driven oscillator in its limit cycle the limit set is a closed curve in the phase space (Fig. 1b).

*Strange attractor.* In the above two examples, the attractors were a point (Fig. 1a), which is a set of dimension zero, and a closed curve (Fig. 1b), which is a set of dimension one. For many other attractors the attracting set can be much more irregular (some would say pathological) and, in fact, can have a dimension that is not an integer. Such sets have been called "fractal" and, when they are attractors, they are called strange attractors. [For a more precise definition see (*1*).] The existence of a strange attractor in a physically interesting model was first demonstrated by Lorenz (*2*).

*Dimension.* There are many definitions of the dimension $d$ (*3*). The simplest is called the box-counting or capacity dimension and is defined as follows:

$$d = \lim_{\epsilon \to 0} \frac{\ln N(\epsilon)}{\ln(1/\epsilon)} \qquad (1)$$

where we imagine the attracting set in the phase space to be covered by small $D$-dimensional cubes of edge length $\epsilon$, with $D$ the dimension of the phase space. $N(\epsilon)$ is the minimum number of such cubes needed to cover the set. For example, for a point attractor (Fig. 1a), $N(\epsilon) = 1$ independent of $\epsilon$, and Eq. 1 yields $d = 0$ (as it should). For a limit cycle attractor, as in Fig. 1b, we have that $N(\epsilon) \sim \ell/\epsilon$, where $\ell$ is the length of the closed curve in the figure (dotted line); hence, for this case, $d = 1$, by Eq. 1. A less trivial example is illustrated in Fig. 2, in the form of a Cantor set. This set is

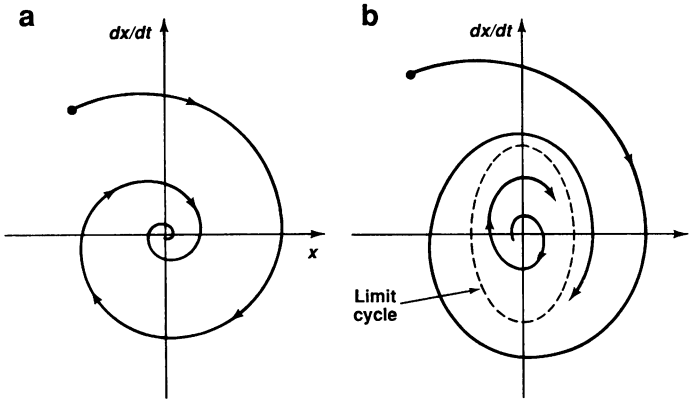


**Fig. 1.** (**a**) Phase-space diagram for a damped harmonic oscillator. (**b**) Phase-space diagram for a system that is approaching a limit cycle.

C. Grebogi is a research scientist at the Laboratory for Plasma and Fusion Energy Studies, E. Ott is a professor in the departments of electrical engineering and physics, and J. A. Yorke is a professor of mathematics and is the director of the Institute for Physical Science and Technology, University of Maryland, College Park, MD 20742.

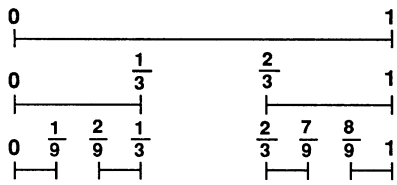


**Fig. 2.** Construction of a Cantor set.

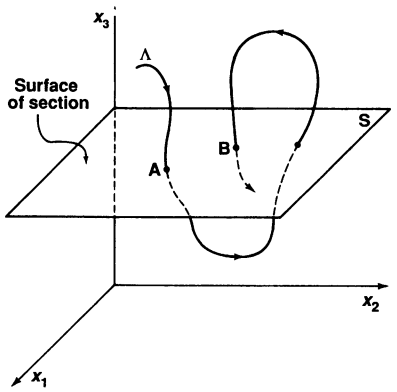


**Fig. 3.** Poincaré surface of section.

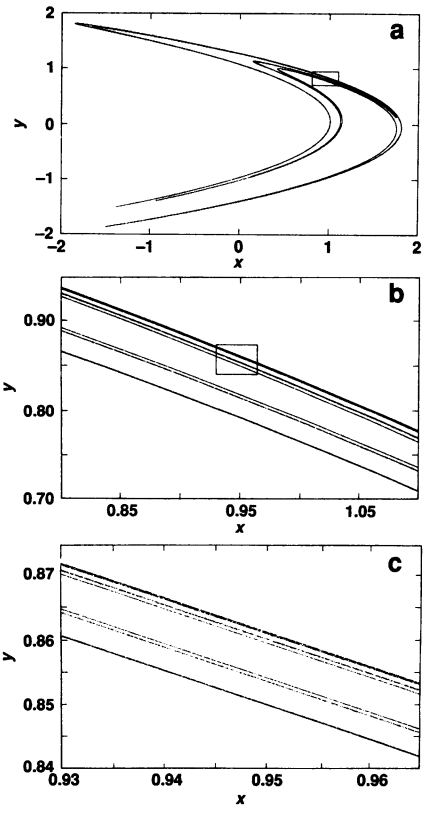


**Fig. 4.** The Hénon chaotic attractor. (**a**) Full set. (**b**) Enlargement of region defined by the rectangle in (a). (**c**) Enlargement of region defined by the rectangle in (b).

formed by taking the line interval from 0 to 1, dividing it in thirds, then discarding the middle third, then dividing the two remaining thirds into thirds and discarding their middle thirds, and so on ad infinitum. The Cantor set is the closed set of points that are left in the limit of this repeated process. If we take $\epsilon = 3^{-n}$ with $n$ an integer, then we see that $N(\epsilon) = 2^n$ and Eq. 1 (in which $\epsilon \to 0$ corresponds to $n \to \infty$) yields $d = (\ln 2)/(\ln 3)$, a number between 0 and 1, hence, a fractal. The topic of the dimension of strange attractors is a large subject on which much research has been done. One of the most interesting aspects concerning dimension arises from the fact that the distribution of points on a chaotic attractor can be nonuniform in a very singular way. In particular, there can be an arbitrarily fine-scaled interwoven structure of regions where orbit trajectories are dense and sparse. Such attractors have been called multifractals and can be characterized by subsidiary quantities that essentially give the dimensions of the dense and sparse regions of the attractor. In this review we shall not attempt to survey this work. Several papers provide an introduction to recent work on the dimension of chaotic attractors (*3–5*).

*Chaotic attractor.* By this term we mean that if we take two typical points on the attractor that are separated from each other by a small distance $\Delta(0)$ at $t = 0$, then for increasing $t$ they move apart exponentially fast. That is, in some average sense $\Delta(t) \sim \Delta(0)\exp(ht)$ with $h > 0$ (where $h$ is called the Lyapunov exponent). Thus a small uncertainty in the initial state of the system rapidly leads to inability to forecast its future. [It is not surprising, therefore, that the pioneering work of Lorenz (*2*) was in the context of meteorology.] It is typically the case that strange attractors are also chaotic [although this is not always so; see (*1, 6*)].

*Dynamical system.* This is a system of equations that allows one, in principle, to predict the future given the past. One example is a system of first-order ordinary differential equations in time, $d\mathbf{x}(t)/dt = \mathbf{G}(\mathbf{x},t)$, where $\mathbf{x}(t)$ is a $D$-dimensional vector and $\mathbf{G}$ is a $D$-dimensional vector function of $\mathbf{x}$ and $t$. Another example is a map.

*Map.* A map is an equation of the form $\mathbf{x}_{t+1} = \mathbf{F}(\mathbf{x}_t)$, where the "time" $t$ is discrete and integer valued. Thus, given $\mathbf{x}_0$, the map gives $\mathbf{x}_1$. Given $\mathbf{x}_1$, the map gives $\mathbf{x}_2$, and so on. Maps can arise in continuous time physical systems in the form of a Poincaré surface of section. Figure 3 illustrates this. The plane $x_3$ = constant is the surface of section (S in the figure), and Λ denotes a trajectory of the system. Every time Λ pierces S going downward (as at points A and B in the figure), we record the coordinates $(x_1,x_2)$. Clearly the coordinates of A uniquely determine those of B. Thus there exists a map, B = F(A), and this map (if we knew it) could be iterated to find all subsequent piercings of S.

## Chaotic Attractors

As an example of a strange attractor consider the map first studied by Hénon (*7*):

$$x_{n+1} = \alpha - x_n^2 + \beta y_n \tag{2}$$

$$y_{n+1} = x_n \tag{3}$$

Figure 4a shows the result of plotting $10^4$ successive points obtained by iterating Eqs. 2 and 3 with parameters $\alpha = 1.4$ and $\beta = 0.3$ (and the initial transient is deleted). The result is essentially a picture of the chaotic attractor. Figure 4, b and c, shows successive enlargements of the small square in the preceding figure. Scale invariant, Cantor set–like structure transverse to the linear structure is evident. This suggests that we may regard the attractor in Fig. 4c, for example, as being essentially a Cantor set of approximately straight parallel lines. In fact, the dimension $d$ in Eq. 1 can be estimated numerically (*8*) to be $d \cong 1.26$ so that the attractor is strange.

As another example consider a forced damped pendulum described by the equation

$$d^2\theta/dt^2 + \nu d\theta/dt + \omega_0^2 \sin\theta = f\cos(\omega t) \tag{4}$$

where $\theta$ is the angle between the pendulum arm and the rest position, $\nu$ is the coefficient of friction, $\omega_0$ is the frequency of natural oscillation, and $f$ is the strength of the forcing. In Eq. 4, the first term represents the inertia of the pendulum, the second term represents friction at the pivot, the third represents the gravitational force, and the right side represents an external sinusoidally varying torque of strength $f$ and frequency $\omega$ applied to the pendulum at the pivot. In Fig. 5a, we plot the Poincaré surface of section of a strange

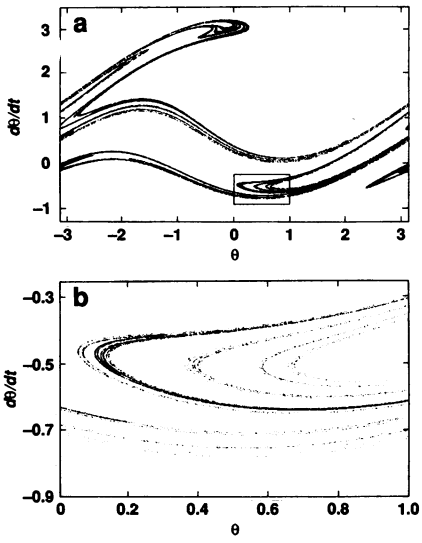


**Fig. 5.** (**a**) Poincaré surface of section of a pendulum strange attractor. (**b**) Enlargement of region defined by rectangle in (a).

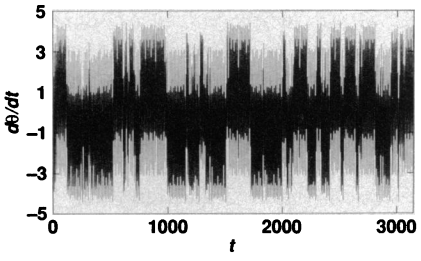


**Fig. 6.** Chaotic time series for pendulum shown as a plot of angular velocity versus time.

attractor for the pendulum, where we choose $\nu = 0.22$, $\omega_0 = 1.0$, $\omega = 1.0$, and $f = 2.7$ in Eq. 4. This surface of section is obtained by plotting 50,000 dots, one dot for every cycle of the forcing term, that is, one dot at every time $t = t_n = 2\pi n$ (where $n$ is an integer). The strange attractor shown in Fig. 5a exhibits a Cantor set–like structure transverse to the linear structure. This is evident in Fig. 5b, which shows an enlargement of the square region in Fig. 5a. The dimension of this strange attractor in the surface of section is $d \cong 1.38$. Figure 6 shows the angular velocity $d\theta/dt$ as a function of $t$ for the parameters of Fig. 5. Note the apparently erratic nature of this plot.

In general, the form of chaotic attractors varies greatly from system to system and even within the same system. This is indicated by the sequence of chaotic attractors shown in Fig. 7. All of these attractors were generated from the same map (*9*),

$$\psi_{n+1} = [\psi_n + \omega_1 + \epsilon P_1(\psi_n,\theta_n)] \bmod 1 \quad (5)$$

$$\theta_{n+1} = [\theta_n + \omega_2 + \epsilon P_2(\psi_n,\theta_n)] \bmod 1 \quad (6)$$

where $P_1$ and $P_2$ are periodic with period one in both their arguments. The $P_1$ and $P_2$ are the same in all of the cases shown in Fig. 7; only the parameters $\omega_1$, $\omega_2$, and $\epsilon$ have been varied. The results show the great variety of form and structure possible in chaotic attractors as well as their aesthetic appeal. Since $\psi$ and $\theta$ may be regarded as angles, Eqs. 5 and 6 are a map on a two-dimensional toroidal surface. [This map is used in (*9*) to study the transition from quasiperiodicity to chaos.]

Because of the exponential divergence of nearby orbits on chaotic attractors, there is a question as to how much of the structure in these pictures of chaotic attractors (Figs. 4, 5, and 7) is an artifact due to chaos-amplified roundoff error. Although a numerical trajectory will diverge rapidly from the true trajectory with the same initial point, it has been demonstrated rigorously (*10*) in important cases [including the Hénon map (*11*)] that there exists a true trajectory with a slightly different initial point that stays near the noisy trajectory for a long time. [For example, for the Hénon map for a typical numerical trajectory computed with 14-digit precision there exists a true trajectory that stays within $10^{-7}$ of the numerical trajectory for $10^7$ iterates (*11*).] Thus we believe that the apparently fractal structure seen in pictures such as Figs. 4, 5, and 7 is real.

## The Evolution of Chaotic Attractors

In dissipative dynamics it is common to find that for some value of a system parameter only a nonchaotic attracting orbit (a limit cycle, for example) occurs, whereas at some other value of the parameter a chaotic attractor occurs. It is therefore natural to ask how the one comes about from the other as the system parameter is varied continuously. This is a fundamental question that has elicited a great deal of attention (*9, 12–19*).

To understand the nature of this question and some of the possible answers to it, we consider Fig. 8a, the so-called bifurcation diagram for the map.

$$x_{n+1} = C - x_n^2 \quad (7)$$

where $C$ is a constant. Figure 8a can be constructed as follows: take $C = -0.4$, set $x_0 = -0.5$, iterate the map 100 times (to eliminate transients), then plot the next 1000 values of $x$; increase $C$ by a small amount, say 0.001, and repeat what was done for $C = -0.4$; increase again, and repeat; and so on, until $C = 2.1$ is reached. We see from Fig. 8a that below a certain value, $C = C_0 = -0.25$, there is no attractor in $-2 < x < 2$. In fact, in this case all orbits go to $x \to -\infty$, hence the absence of points on the plot. This is also true for $C$ above the "crisis value" $C_c = 2.0$. Between these two values there is an attractor. As $C$ is increased we have an attracting orbit of "period one," which, at $C = 0.75$, bifurcates to a period-two attracting orbit ($x_\alpha \to x_\beta \to x_\alpha \to x_\beta \to \cdots$), which then bifurcates (at $C = 1.25$) to a period-four orbit ($x_a \to x_b \to x_c \to x_d \to x_a \to x_b \to x_c \to x_d \to x_a \to \cdots$). In fact, there are an infinite number of such bifurcations of period $2^n$ to period $2^{n+1}$ orbits, and these accumulate as $n \to \infty$ at a finite value of $C$, which we denote $C_\infty$ (from Fig. 8a, $C_\infty \cong 1.4$). [The practical importance of this phenomenology was emphasized early on by May (*12*).]

What is the situation for $C_\infty < C < C_c$? Numerically what one sees is that for many $C$ values in this range the orbits appear to be chaotic, whereas for others there are periodic orbits. For example, Fig. 8b shows an enlargement of Fig. 8a for $C$ in the range $1.72 < C < 1.82$. We see what appear to be chaotic orbits below $C = C_0^{(3)} = 1.75$. However, just above this value, a period-three orbit appears, supplanting the chaos. The period-three orbit then goes through a period-doubling cascade, becomes chaotic, widens into a three-piece chaotic attractor, and then finally at $C = C_c^{(3)} \cong 1.79$ widens back into a single chaotic band. We call the region $C_0^{(3)} < C < C_c^{(3)}$ a period-three window. (Such windows, but of higher period, appear throughout the region $C_\infty < C < C_c$, but are not as discernible in Fig. 8a because they are much narrower than the period-three window.)

An infinite period-doubling cascade is one way that a chaotic attractor can come about from a nonchaotic one (*13*). There are also two other possible routes to chaos exemplified in Fig. 8, a and b. These are the intermittency route (*14*) and the crisis route (*15*).

*Intermittency.* Consider Fig. 8b. For $C$ just above $C_0^{(3)}$ there is a period-three orbit. For $C$ just below $C_0^{(3)}$ there appears to be a chaotic orbit. To understand the character of this transition it is useful to examine the chaotic orbit for $C$ just below $C_0^{(3)}$. The character of this orbit is as follows: The orbit appears to be a period-three orbit for long stretches of time after which there is a short

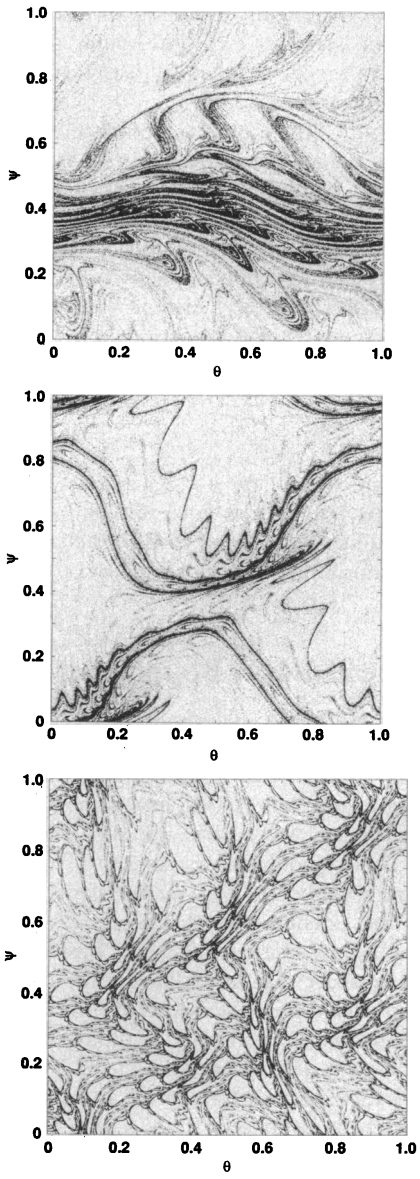


**Fig. 7.** Sequence of chaotic attractors for system represented by Eqs. 5 and 6. Plot shows iterated mapping on a torus for different values of $\omega_1$, $\omega_2$, and $\epsilon$. (**Top**) $\omega_1 = 0.54657$, $\omega_2 = 0.36736$, and $\epsilon = 0.75$. (**Center**) $\omega_1 = 0.45922$, $\omega_2 = 0.53968$, and $\epsilon = 0.50$. (**Bottom**) $\omega_1 = 0.41500$, $\omega_2 = 0.73500$, and $\epsilon = 0.60$.

burst (the "intermittent burst") of chaotic-like behavior, followed by another long stretch of almost period-three behavior, followed by a chaotic burst, and so on. As $C$ approaches $C_0^{(3)}$ from below, the average duration of the long stretches between the intermittent bursts becomes longer and longer (*14*), approaching infinity and proportional to $(C_0^{(3)} - C)^{-1/2}$ as $C \rightarrow C_0^{(3)}$. Thus the pure period-three orbit appears at $C = C_0^{(3)}$. Alternatively we may say that the attracting periodic attractor of period three is converted to a chaotic attractor as the parameter $C$ decreases through the critical value $C_0^{(3)}$. It should be emphasized that, although our illustration of the transition to chaos by way of intermittency is within the context of the period-three window of the quadratic map given by Eq. 7, this phenomenon (as well as period-doubling cascades and crises) is very general; in other systems it occurs for other periods (period one, for example) in easily observable form.

*Crises.* From Fig. 8a we see that there is a chaotic attractor for $C < C_c = 2$, but no chaotic attractor for $C > C_c$. Thus, as $C$ is lowered through $C_c$, a chaotic attractor is born. How does this occur? Note that at $C = C_c$ the chaotic orbit occupies the interval $-2 \leq x \leq 2$. If $C$ is just slightly larger than $C_c$, an orbit with initial condition in the interval $-2 < x < 2$ will typically follow a chaotic-like path for a finite time, after which it finds its way out of the interval $-2 \leq x \leq 2$, and then rapidly begins to move to large negative $x$ values (that is, it begins to approach $x = -\infty$). This is called a chaotic transient (*15*). The length of a chaotic transient will depend on the particular initial condition chosen. One can define a mean transient duration by averaging over, for example, a uniform distribution of initial conditions in the interval $-2 < x < 2$. For the quadratic map, this average duration is

$$\tau \sim 1/(C - C_c)^{\gamma} \tag{8}$$

with the exponent $\gamma$ given by $\gamma = 1/2$. Thus as $C$ approaches $C_c$ from above, the lifetime of a chaotic transient goes to infinity and the transient is converted to a chaotic attractor for $C < C_c$. Again, this type of phenomenon occurs widely in chaotic systems. For example, the model of Lorenz (*2*) for the nonlinear evolution of the Rayleigh-Bénard instability of a fluid subjected to gravity and heated from below has a chaotic onset of the crisis type and an accompanying chaotic transient. In that case, $\gamma$ in Eq. 8 is $\gamma \sim 4$ (*20*). In addition, a theory for determining the exponent $\gamma$ for two-dimensional maps and systems such as the forced damped pendulum has recently been published (*21*). Thus we have seen that the period doubling, intermittency, and crisis routes to chaos are illustrated by the simple quadratic map (Eq. 7).

We emphasize that, although a map was used for illustrating these routes, all of these phenomena are present in continuous-time systems and have been observed in experiments. As an example of chaotic transitions in a continuous time system, we consider the set of three autonomous ordinary differential equations studied by Lorenz (*2*) as a model of the Rayleigh-Bénard instability,

$$dx/dt = Py - Px \tag{9}$$

$$dy/dt = -xz + rx - y \tag{10}$$

$$dz/dt = xy - bz \tag{11}$$

where $P$ and $b$ are adjustable parameters. Fixing $P = 10$ and $b = 8/3$ and varying the remaining parameter, $r$, we obtain numerical solutions that are clear examples of the intermittency and crisis types of chaotic transitions discussed above. We illustrate these in Fig. 9, a through d; the behavior of this system is as follows:

1) For $r$ between 166.0 and 166.2 there is an intermittency transition from a periodic attractor ($r = 166.0$, Fig. 9a) to a chaotic attractor ($r = 166.2$, Fig. 9b) with intermittent turbulent bursts. Between the bursts there are long stretches of time for which the orbit oscillates in nearly the same way as for the periodic attractor (*14*) (Fig. 9a).

2) For a range of $r$ values below $r = 24.06$ there are two periodic attractors, that represent clockwise and counterclockwise convections. For $r$ slightly above 24.06, however, there are three attractors, one that is chaotic (shown in the phase space trajectory in Fig. 9c), whereas the other two attractors are the previously mentioned periodic attractors. The chaotic attractor comes into existence as $r$ increases through $r = 24.06$ by conversion of a chaotic transient. Figure 9d shows an orbit in phase space executing a chaotic transient before settling down to its final resting place at one of the periodic attractors. Note the similarity of the chaotic transient trajectory in Fig. 9d with the chaotic trajectory in Fig. 9c.

The various routes to chaos have also received exhaustive experimental support. For instance, period-doubling cascades have been observed in the Rayleigh-Bénard convection (*22, 23*), in nonlinear circuits (*24*), and in lasers (*25*); intermittency has been observed in the Rayleigh-Bénard convection (*26*) and in the Belousov-Zhabotinsky reaction (*27*); and crises have been observed in nonlinear circuits (*28–30*), in the Josephson junction (*31*), and in lasers (*32*).

Finally, we note that period doubling, intermittency, and crises do not exhaust the possible list of routes to chaos. (Indeed, the

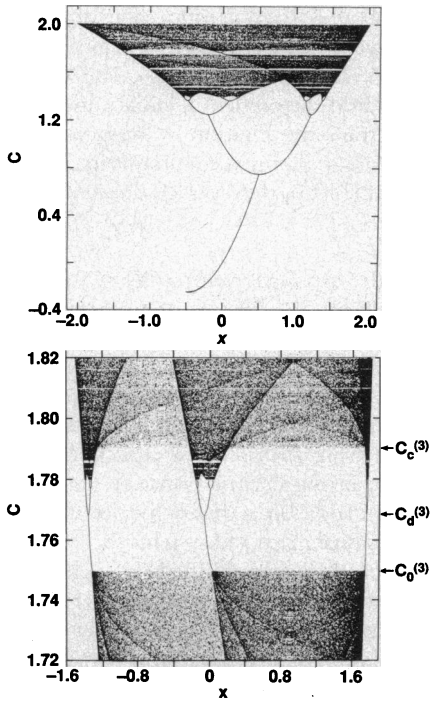


**Fig. 8.** (**Top**) Bifurcation diagram for the quadratic map. (**Bottom**) Period-three window for the quadratic map.

routes are not all known.) In particular, chaotic onsets involving quasiperiodicity have not been discussed here (*9, 16, 18*).

## Universality

Universality refers to the fact that systems behave in certain quantitative ways that depend not on the detailed physics or model description but rather only on some general properties of the system. Universality has been examined by renormalization group (*33*) techniques developed for the study of critical phenomena in condensed matter physics. In the context of dynamics, Feigenbaum (*13*) was the first to apply these ideas, and he has extensively developed them, particularly for period doubling for dissipative systems. [See (*17*) for a collection of papers on universality in nonlinear dynamics.] For period doubling in dissipative systems, results have been obtained on the scaling behavior of power spectra for time series of the dynamical process (*34*), on the effect of noise on period doubling (*35*), and on the dependence of the Lyapunov exponent (*36*) on a system parameter. Applications of the renormalization group have also been made to intermittency (*19, 37*), and the breakdown of quasiperiodicity in dissipative (*18*) and conservative (*38*) systems.

As examples, two "universal" results can be stated within the context of the bifurcation diagrams (Fig. 8, a and b). Let $C_n$ denote the value of $C$ at which a period $2^n$ cycle period doubles to become a period $2^{n+1}$ cycle. Then, for the bifurcation diagram in Fig. 8a, one obtains

$$\lim_{n\to\infty} \frac{C_n - C_{n-1}}{C_{n+1} - C_n} = 4.669201\ldots \qquad (12)$$

The result given in Eq. 12 is not restricted to the quadratic map. In fact, it applies to a broad class of systems that undergo period doubling cascades (*13, 39*). In practice such cascades are very common, and the associated universal numbers are observed to be well approximated by means of fairly low order bifurcations (for example, $n$ = 2,3,4). This scaling behavior has been observed in many experiments, including ones on fluids, nonlinear circuits, laser systems, and so forth. Although universality arguments do not explain why cascades must exist, such explanations are available from bifurcation theory (*40*).

Figure 8b shows the period-three window within the chaotic range of the quadratic map. As already mentioned, there are an infinite number of such periodic windows. [In fact, they are generally believed to be dense in the chaotic range. For example, if $k$ is prime, there are $(2^k - 2)/(2k)$ period-$k$ windows.] Let $C_0^{(k)}$ and $C_c^{(k)}$ denote the upper and lower values of $C$ bounding the period-$k$ window and let $C_d^{(k)}$ denote the value of $C$ at which the period-$k$ attractor bifurcates to period $2k$. Then we have that, for typical $k$ windows (*41*).

$$\lim_{k\to\infty} \frac{C_c^{(k)} - C_0^{(k)}}{C_d^{(k)} - C_0^{(k)}} \to 9/4 \qquad (13)$$

In fact, even for the $k$ = 3 window (Fig. 8b) the 9/4 value is closely approximated (it is 9/4 − 0.074 . . .). This result is universal for one-dimensional maps (and possibly more generally for any chaotic dynamical process) with windows.

## Fractal Basin Boundaries

In addition to chaotic attractors, there can be sets in phase space on which orbits are chaotic but for which points near the set move away from the set. That is, they are repelled. Nevertheless, such chaotic repellers can still have important macroscopically observable effects, and we consider one such effect (*42, 43*) in this section.

Typical nonlinear dynamical systems may have more than one time-asymptotic final state (attractor), and it is important to consider the extent to which uncertainty in initial conditions leads to uncertainty in the final state. Consider the simple two-dimensional phase space diagram schematically depicted in Fig. 10. There are two attractors denoted A and B. Initial conditions on one side of the boundary, Σ, eventually asymptotically approach B; those on the other side of Σ eventually go to A. The region to the left or right of Σ is the basin of attraction for attractor A or B, respectively, and Σ is the basin boundary. If the initial conditions are uncertain by an amount ϵ, then for those initial conditions within ϵ of the boundary we cannot say a priori to which attractor the orbit eventually tends.

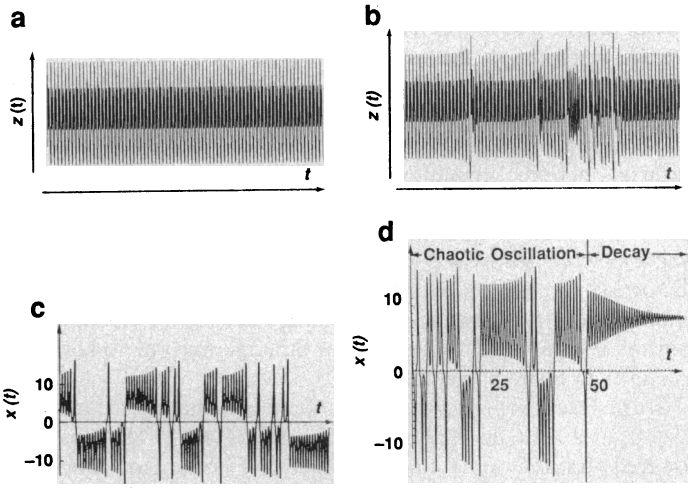


**Fig. 9.** Intermittency, crisis, and period doubling in continuous time systems. Intermittency in the Lorenz equations (**a**) $r$ = 166.0; (**b**) $r$ = 166.2. Crisis transition to a chaotic attractor in the Lorenz equations: (**c**) $r$ = 28; (**d**) $r$ = 22.

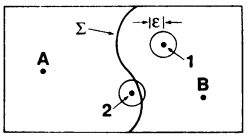


**Fig. 10.** A region of phase space divided by the basin boundary Σ into basins of attraction for the two attractors A and B. Points 1 and 2 are initial conditions with error $\epsilon$.

For example, in Fig. 10, points 1 and 2 are initial conditions with an uncertainty $\epsilon$. The orbit generated by initial condition 1 is attracted to attractor B. Initial condition 2, however, is uncertain in the sense that the orbit generated by 2 may be attracted either to A or B. In particular, consider the fraction of the uncertain phase space volume within the rectangle shown and denote this fraction $f$. For the case shown in Fig. 10, we clearly have $f \sim \epsilon$. The main point we wish to make in what follows is that, from the point of view of prediction, much worse scalings of $f$ with $\epsilon$ frequently occur in nonlinear dynamics. Namely, the fraction can scale as

$$f \sim \epsilon^{\alpha} \tag{14}$$

with the "uncertainty exponent" $\alpha$ satisfying $\alpha < 1$ (*42, 43*). In fact, $\alpha << 1$ is fairly common. In such a case, a substantial reduction in the initial condition uncertainty, $\epsilon$, yields only a relatively small decrease in the uncertainty of the final state as measured by $f$.

Although $\alpha$ is equal to unity for simple basin boundaries, such as that depicted in Fig. 10, boundaries with noninteger (fractal) dimension also occur. We use here the capacity definition of dimension, Eq. 1. In general, since the basin boundary divides the phase space, its dimension $d$ must satisfy $d \geq D - 1$, where $D$ is the dimension of the phase space. It can be proven that the following relation between the index $\alpha$ and the basin boundary dimension holds (*42, 43*)

$$\alpha = D - d \tag{15}$$

For a simple boundary, such as that depicted in Fig. 10, we have $d = D - 1$, and Eq. 15 then gives $\alpha = 1$, as expected. For a fractal basin boundary, $d > D - 1$, and Eq. 15 gives $\alpha < 1$.

We now illustrate the above with a concrete example. Consider the forced damped pendulum as given by Eq. 4. For parameter values $\nu = 0.2$, $\omega_0 = 1.0$, $\omega = 1.0$, and $f = 2.0$, we find numerically that the only attractors in the surface of section ($\theta$, $d\theta/dt$) are the fixed points $(-0.477, -0.609)$ and $(-0.471, 2.037)$. They represent solutions with average counterclockwise and clockwise rotation at the period of the forcing. The cover shows a computer-generated picture of the basins of attraction for the two fixed point attractors. Each initial condition in a 1024 by 1024 point grid is integrated until it is close to one of the two attractors (typically 100 cycles). If an orbit goes to the attractor at $\theta = -0.477$, a blue dot is plotted at the corresponding initial condition. If the orbit goes to the other attractor, a red dot is plotted. Thus the blue and red regions are essentially pictures of the basins of attraction for the two attractors to the accuracy of the grid of the computer plotter. Fine-scale structure in the basins of attraction is evident. This is a consequence of the Cantor-set nature of the basin boundary. In fact, magnifications of the basin boundary show that, as we examine it on a smaller and smaller scale, it continues to have structure.

We now wish to explore the consequences for prediction of this infinitely fine-scaled structure. To do this, consider an initial condition ($\theta$, $d\theta/dt$). What is the effect of a small change $\epsilon$ in the $\theta$-coordinate? Thus we integrate the forced pendulum equation with the initial conditions ($\theta$, $d\theta/dt$), ($\theta$, $d\theta/dt + \epsilon$), and ($\theta$, $d\theta/dt - \epsilon$) until they approach one of the attractors. If either or both of the perturbed initial conditions yield orbits that do not approach the same attractor as the unperturbed initial condition, we say that ($\theta$, $d\theta/dt$) is uncertain. Now we randomly choose a large number of initial conditions and let $\hat{f}$ denote the fraction of these that we find to be uncertain. As a result of these calculations, we find that $\hat{f} \sim \epsilon^{\hat{\alpha}}$ where $\hat{\alpha} \cong 0.275 \pm 0.005$. If we assume that $\hat{f}$, determined in the way stated above, is approximately proportional to $f$ [there is some support for this conjecture from theoretical work (*44*)], then $\alpha = \hat{\alpha}$. Thus, from Eq. 15, the dimension of the basin boundary is $d \cong 1.725 \pm 0.005$. We conclude, from Eq. 14, that in this case if we are to gain a factor of 2 in the ability to predict the asymptotic final state of the system, it is necessary to increase the accuracy in the measurement of the initial conditions by a factor substantially greater than 2 (namely by $2^{1/0.275} \cong 10$). Hence, fractal basin boundaries ($\alpha < 1$) represent an obstruction to predictability in nonlinear dynamics.

Some representative works on fractal basin boundaries, including applications, are listed in (*42–47*). Notable basic questions that have recently been answered are the following:

1) How does a nonfractal basin boundary become a fractal basin boundary as a parameter of the system is varied (*45*)? This question is similar, in spirit, to the question of how chaotic attractors come about.

2) Can fractal basin boundaries have different dimension values in different regions of the boundary, and what boundary structures lead to this situation? This question is addressed in (*46*) where it is shown that regions of different dimension can be intertwined on an arbitrarily fine scale.

3) What are the effects of a fractal basin boundary when the system is subject to noise? This has been addressed in the Josephson junction experiments of (*31*).

## Conclusion

Chaotic nonlinear dynamics is a vigorous, rapidly expanding field. Many important future applications are to be expected in a variety of areas. In addition to its practical aspects, the field also has fundamental implications. According to Laplace, determination of the future depends only on the present state. Chaos adds a basic new aspect to this rule: small errors in our knowledge can grow exponentially with time, thus making the long-term prediction of the future impossible.

Although the field has advanced at a great rate in recent years, there is still a wealth of challenging fundamental questions that have yet to be adequately dealt with. For example, most concepts developed so far have been discovered in what are effectively low-dimensional systems; what undiscovered important phenomena will appear only in higher dimensions? Why are transiently chaotic motions so prevalent in higher dimensions? In what ways is it possible to use the dimension of a chaotic attractor to determine the dimension of the phase space necessary to describe the dynamics? Can renormalization group techniques be extended past the borderline of chaos into the strongly chaotic regime? These are only a few questions. There are many more, and probably the most important questions are those that have not yet been asked.

### REFERENCES AND NOTES

1. C. Grebogi, E. Ott, S. Pelikan, J. A. Yorke, *Physica* **13D**, 261 (1984).
2. E. N. Lorenz, *J. Atmos. Sci.* **20**, 130 (1963).
3. J. D. Farmer, E. Ott, J. A. Yorke, *Physica* **7D**, 153 (1983).
4. J. Kaplan and J. A. Yorke, *Lecture Notes in Mathematics No. 730* (Springer-Verlag, Berlin, 1978), p. 228; L. S. Young, *Ergodic Theory Dyn. Syst.* **1**, 381 (1981).
5. P. Grassberger and I. Procaccia, *Phys. Rev. Lett.* **50**, 346 (1983); H. G. E. Hentschel and I. Procaccia, *Physica* **8D**, 435 (1983); P. Grassberger, *Phys. Lett.* **A97**, 227 (1983); T. C. Halsey *et al.*, B. I. Shraiman, *Phys. Rev. A* **33**, 1141 (1986); C. Grebogi, E. Ott, J. A. Yorke, *ibid.* **36**, 3522 (1987).
6. A. Bondeson *et al.*, *Phys. Rev. Lett.* **55**, 2103 (1985); F. J. Romeiras, A. Bondeson, E. Ott, T. M. Antonsen, C. Grebogi, *Physica* **26D**, 277 (1987).
7. M. Hénon, *Commun. Math. Phys.* **50**, 69 (1976).
8. D. A. Russell, J. D. Hanson, E. Ott, *Phys. Rev. Lett.* **45**, 1175 (1980).
9. C. Grebogi, E. Ott, J. A. Yorke, *Physica* **15D**, 354 (1985).

10. D. V. Anosov, *Proc. Steklov Ins. Math.* **90** (1967); R. Bowen, *J. Differ. Equations* **18**, 333 (1975).
11. S. M. Hammel, J. A. Yorke, C. Grebogi, *J. Complexity*, **3**, 136 (1987).
12. R. M. May, *Nature (London)* **261**, 459 (1976).
13. M. J. Feigenbaum, *J. Stat. Phys.* **19**, 25 (1978).
14. Y. Pomeau and P. Manneville, *Commun. Math. Phys.* **74**, 189 (1980).
15. C. Grebogi, E. Ott, J. A. Yorke, *Physica* **7D**, 181 (1983).
16. D. Ruelle and F. Takens, *Commun. Math. Phys.* **20**, 167 (1971).
17. P. Cvitanovic, Ed. *Universality in Chaos* (Hilger, Bristol, 1984).
18. For example, S. J. Shenker, *Physica* **5D**, 405 (1982); K. Kaneko, *Progr. Theor. Phys.* **71**, 282 (1984); M. J. Feigenbaum, L. P. Kadanoff, S. L. Shenker, *Physica* **5D**, 370 (1982); D. Rand, S. Ostlund, J. Sethna, E. Siggia, *Physica* **8D**, 303 (1983); S. Kim and S. Ostlund, *Phys. Rev. Lett.* **55**, 1165 (1985); D. K. Umberger, J. D. Farmer, I. I. Satija, *Phys. Lett. A* **114**, 341 (1986); P. Bak, T. Bohr, M. H. Jensen, *Phys. Scr.* **T9**, 50 (1985); P. Bak, *Phys. Today* **39** (No. 12), 38 (1987).
19. J. E. Hirsch, M. Nauenberg, D. J. Scalapino, *Phys. Lett. A* **87**, 391 (1982).
20. J. A. Yorke and E. D. Yorke, *J. Stat. Phys.* **21**, 263 (1979); in *Topics in Applied Physics* (Springer-Verlag, New York, 1981), vol. 45, p. 77.
21. C. Grebogi, E. Ott, J. A. Yorke, *Phys. Rev. Lett.* **57**, 1284 (1986).
22. A. Libchaber and J. Maurer, *J. Phys. (Paris)* **41**, C3-51 (1980); A. Libchaber, C. Laroche, S. Fauve, *J. Phys. (Paris) Lett.* **43**, L211 (1982).
23. J. P. Gollub, S. V. Benson, J. F. Steinman, *Ann. N.Y. Acad. Sci.* **357**, 22 (1980); M. Giglio, S. Musazzi, U. Perini, *Phys. Rev. Lett.* **47**, 243 (1981).
24. P. S. Linsay, *Phys. Rev. Lett.* **47**, 1349 (1981).
25. F. T. Arecchi, R. Meucci, G. Puccioni, J. Tredicce, *ibid.* **49**, 1217 (1982).
26. M. Dubois, M. A. Rubio, P. Bergé, *ibid.* **51**, 1446 (1983).
27. J. C. Roux, P. DeKepper, H. L. Swinney, *Physica* **7D**, 57 (1983).
28. C. Jeffries and J. Perez, *Phys. Rev. A* **27**, 601 (1983); S. K. Brorson, D. Dewey, P. S. Linsay, *ibid.* **28**, 1201 (1983).
29. H. Ikezi, J. S. deGrasse, T. H. Jensen, *ibid.* **28**, 1207 (1983).
30. R. W. Rollins and E. R. Hunt, *ibid.* **29**, 3327 (1984).
31. M. Iansiti *et al.*, *Phys. Rev. Lett.* **55**, 746 (1985).
32. D. Dangoisse, P. Glorieux, D. Hannequin, *ibid.* **57**, 2657 (1986).
33. K. G. Wilson and J. Kogut, *Phys. Rep. C* **12**, 75 (1974); B. Hu, *ibid.* **91**, 233 (1982).
34. M. J. Feigenbaum, *Phys. Lett. A* **74**, 375 (1979); R. Brown, C. Grebogi, E. Ott, *Phys. Rev. A* **34**, 2248 (1986); M. Nauenberg and J. Rudnick, *Phys. Rev. B* **24**, 493 (1981); B. A. Huberman and A. B. Zisook, *Phys. Rev. Lett.* **46**, 626 (1981); J. D. Farmer, *ibid.* **47**, 179 (1981).
35. J. Crutchfield, M. Nauenberg, J. Rudnick, *Phys. Rev. Lett.* **46**, 933 (1981); B. Shraiman, C. E. Wayne, P. C. Martin, *ibid.*, p. 935.
36. B. A. Huberman and J. Rudnick, *ibid.* **45**, 154 (1980).
37. B. Hu and J. Rudnick, *ibid.* **48**, 1645 (1982).
38. L. P. Kadanoff, *ibid.* **47**, 1641 (1981); D. F. Escande and F. Doveil, *J. Stat. Phys.* **26**, 257 (1981); R. S. MacKay, *Physica* **7D**, 283 (1983).
39. P. Collet, J. P. Eckmann, O. E. Lanford III, *Commun. Math. Phys.* **76**, 211 (1980).
40. J. A. Yorke and K. A. Alligood, *ibid.* **100**, 1 (1985).
41. J. A. Yorke, C. Grebogi, E. Ott, L. Tedeschini-Lalli, *Phys. Rev. Lett.* **54**, 1095 (1985).
42. C. Grebogi, S. W. McDonald, E. Ott, J. A. Yorke, *Phys. Lett. A* **99**, 415 (1983).
43. S. W. McDonald, C. Grebogi, E. Ott, J. A. Yorke, *Physica* **17D**, 125 (1985).
44. S. Pelikan, *Trans. Am. Math. Soc.* **292**, 695 (1985).
45. C. Grebogi, E. Ott, J. A. Yorke, *Phys. Rev. Lett.* **56**, 1011 (1986); *Physica* **24D**, 243 (1987); F. C. Moon and G.-X. Li, *Phys. Rev. Lett.* **55**, 1439 (1985).
46. C. Grebogi, E. Kostelich, E. Ott, J. A. Yorke, *Phys. Lett.* **A118**, 448 (1986); *Physica* **25D**, 347 (1987); C. Grebogi, E. Ott, J. A. Yorke, H. E. Nusse, *Ann. N.Y. Acad. Sci.* **497**, 117 (1987).
47. C. Mira, *C. R. Acad. Sci.* **288A**, 591 (1979); C. Grebogi, E. Ott, J. A. Yorke, *Phys. Rev. Lett.* **50**, 935 (1983); R. G. Holt and I. B. Schwartz, *Phys. Lett.* **A105**, 327 (1984); I. B. Schwartz, *ibid.* **106**, 339 (1984); I. B. Schwartz, *J. Math. Biol.* **21**, 347 (1985); S. Takesue and K. Kaneko, *Progr. Theor. Phys.* **71**, 35 (1984); O. Decroly and A. Goldbeter, *Phys. Lett.* **A105**, 259 (1984); E. G. Gwinn and R. M. Westervelt, *Phys. Rev. Lett.* **54**, 1613 (1985); *Phys. Rev. A* **33**, 4143 (1986); Y. Yamaguchi and N. Mishima, *Phys. Lett.* **A109**, 196 (1985); M. Napiorkowski, *ibid.* **113**, 111 (1985); F. T. Arecchi, R. Badii, A. Politi, *Phys. Rev. A* **32**, 402 (1985); S. W. McDonald, C. Grebogi, E. Ott, J. A. Yorke, *Phys. Lett.* **A107**, 51 (1985); J. S. Nicolis and I. Tsuda, in *Simulation, Communication, and Control*, S. G. Tzafestas, Ed. (North-Holland, Amsterdam, 1985); J. S. Nicolis, *Rep. Prog. Phys.* **49**, 1109 (1986); J. S. Nicolis, *Kybernetes* **14**, 167 (1985).
48. This work was supported by the Air Force Office of Scientific Research, the U.S. Department of Energy, the Defense Advanced Research Projects Agency, and the Office of Naval Research.

# Actin Polymerization and ATP Hydrolysis

EDWARD D. KORN,* MARIE-FRANCE CARLIER, DOMINIQUE PANTALONI

**F-actin is the major component of muscle thin filaments and, more generally, of the microfilaments of the dynamic, multifunctional cytoskeletal systems of nonmuscle eukaryotic cells. Polymeric F-actin is formed by reversible noncovalent self-association of monomeric G-actin. To understand the dynamics of microfilament systems in cells, the dynamics of polymerization of pure actin must be understood. The following model has emerged from recent work. During the polymerization process, adenosine 5′-triphosphate (ATP) that is bound to G-actin is hydrolyzed to adenosine 5′-diphosphate (ADP) that is bound to F-actin. The hydrolysis reaction occurs on the F-actin subsequent to the polymerization reaction in two steps: cleavage of ATP followed by the slower release of inorganic phosphate ($P_i$). As a result, at high rates of filament growth a transient cap of ATP-actin subunits exists at the ends of elongating filaments, and at steady state a stabilizing cap of ADP · $P_i$-actin subunits exists at the barbed ends of filaments. Cleavage of ATP results in a highly stable filament with bound ADP · $P_i$, and release of $P_i$ destabilizes the filament. Thus these two steps of the hydrolytic reaction provide potential mechanisms for regulating the monomer-polymer transition.**

ACTIN, WHICH IS ONE OF THE TWO MAJOR PROTEINS OF muscle, occurs in every eukaryotic cell, in which it can account for more than 20% of the total cell protein (*1*). In addition to being one of the more abundant proteins in nature, actin is also one of the most highly conserved proteins. From amoebas to humans, actins are about 95% identical in amino acid sequence (*2*); yeast and soybean actins (*3*) are about 85% and *Tetrahymena* actin (*4*) is about 75% identical to muscle actins. Many of the substitutions that do occur are chemically conservative (for example, aspartate for glutamate) and restricted to a few regions of the polypeptide chain (*2–4*). Both its widespread occurrence and the evolutionary stability of its primary structure suggest the fundamental biological importance of actin.

Actin is a bilobed, approximately pear-shaped molecule (*5*) that consists of a single polypeptide chain of 42,000 daltons (*1, 2*). Monomeric at nonphysiologically low ionic strength, pure G-actin polymerizes through reversible noncovalent associations (*1, 6*) into filaments of F-actin that contain thousands of protomers (*7*), when either the $Mg^{2+}$ concentration or the ionic strength is closer to

E. D. Korn is chief of the Laboratory of Cell Biology, National Heart, Lung, and Blood Institute, National Institutes of Health, Bethesda, MD 20892. M.-F. Carlier and D. Pantaloni are at the Laboratoire d'Enzymologie, CNRS, 91190 Gif-sur-Yvette, France.

*To whom correspondence should be addressed.